Research Article

Saib Thiab Alwan, Abbas Al-Bawee, and Ahmed A. A. G. Alrubaiy*

Effective thickness of gallium arsenide on the transverse electric and transverse magnetic modes

https://doi.org/10.1515/cls-2025-0033
received February 04, 2025; accepted June 16, 2025

Abstract: The aim of this work is to investigate gallium arsenide, a particular kind of semiconductor. The study employs a three-layer asymmetric slab waveguide structure, where a thin gallium arsenide (GaAs) film is deposited on a glass substrate, and above the film is a dielectric cladding, such as air. To enable complete internal reflection at the interfaces, the guiding slab's index of refraction has to be greater than that of the cover material (cladding) or the substrate material. Further investigated are the effects of the thickness of GaAs on transverse electric/transverse magnetic (TE/TM) propagation modes typically. Every method was shown with specific settings. The thickness of GaAs affects the number of TE/TM modes. Cut-off wavenumber and attenuation decrease for a particular applied wavelength (0.6328 μm) due to decreasing propagation wavenumber. Simulation findings clearly reveal that the basic mode has the biggest incidence angle and lowest penetration depth; the highest mode has the incidence angle very near the critical angle and the best penetration depth. The design of integrated optical devices depends on optical waveguides, which calls for consistent and accurate findings for defining the waveguide's properties prior to manufacturing.

Keywords: terahertz frequency range, waveguide, a symmetric dielectric slab, TE and TM modes, microwave propagation, gallium arsenide

*** Corresponding author: Ahmed A. A. G. Alrubaiy,** Department of Materials, College of Engineering, University of Diyala, Diyala, Iraq, e-mail: Ahmed_Ali_eng@uodiyala.edu.iq
Saib Thiab Alwan: Department of Materials, College of Engineering, University of Diyala, Diyala, Iraq, e-mail: Saib_alwan_eng@uodiyala.edu.iq
Abbas Al-Bawee: Department of Materials, College of Engineering, University of Diyala, Diyala, Iraq, e-mail: abbas_taha_eng@uodiyala.edu.iq

1 Introduction

To figure out the optical properties of gallium arsenide (GaAs)-based devices like optical limiters, mode-matching metamaterials, and photonic crystals, it is important to know how thick the material is in both the transverse electric (TE) and transverse magnetic (TM) modes. It is common for "effective thickness" in the TE mode to mean the thickness of the GaAs layer that would cause the same phase shift as the real GaAs layer, taking into account the change in the refractive index and the applied electric field along the growth direction [1]. The study investigates the impact of layer thickness on TE/TM mode behavior in GaAs-based slab waveguides. It focuses on the influence of GaAs thickness on propagation modes, cut-off wavenumbers, attenuation and total internal reflection angles. The research focuses on the design, optimization and fabrication of slab waveguides in III–V semiconductor materials. Despite extensive studies there is a lack of research on the direct relationship between material thickness and the distribution, cutoff, and attenuation behavior of TE/TM modes, particularly in symmetric slab configurations.

Waveguide sensors work by means of the evanescent field existing in the cladding layer, where the analyte to be detected is found. The thickness of the guiding layer and the refractive indices of every media component affect the effective refractive index of the guided mode detected in a waveguide structure. Consequently, the effective refractive index of the light-guided mode varies with any change in the refractive index of the analyte within the cladding layer. Kołacz *et al.* [2] studied TE/TM modes in liquid crystal-clad waveguides, focusing on material-cladding interactions and mode confinement and dispersion, aligning with our analysis of air-clad GaAs waveguides, where the cladding (air) significantly influences mode confinement and attenuation behavior.

Mechanical characteristics have been much improved in material science thanks to recent developments in which the creative molten Bi-Ga austempering process

stands out. These developments are on par with the advances in GaAs-based optical devices, which have attained better performance and lifetime [3]. Many investigations have produced a comprehensive collection of hypotheses that enable us to better grasp the behavior of TE and TM modes in slab waveguides, particularly those grounded on GaAs. However, a systematic analysis of how GaAs thickness directly influences the cutoff wavenumbers, attenuation, and mode confinement in asymmetric slab waveguides remains underexplored, particularly for applications in terahertz and integrated photonics. These works tackle the numerical methods for mode equation solving, the impact of waveguide properties on mode profiles, and mode equation derivation. Recent advancements in GaAs-based waveguide design (Midolo *et al.* [1], Chen and Uddin [4]) emphasize the need for precise thickness control, yet quantitative comparisons between TE/TM mode behaviors across varying GaAs thicknesses are limited. Modal interactions in optical systems can be optimized using polarization techniques, as explored by He *et al.* [5]. By using bidirectional signals with orthogonal TE/TM polarizations, angular resolution is improved. This approach aligns with the draft's analysis of TE/TM mode behavior, providing a comparative perspective on managing orthogonal modes. Alwan *et al.* [6] investigated the asymmetric slab waveguides with great attention for mode count and propagation characteristics. Crucially for knowledge of the behavior of TE and TM modes in GaAs-based waveguides, they explored how the thickness of the guiding layer influences mode profiles and attenuation. By means of a theoretical investigation of slab waveguides, Chen and Uddin [4] derived mode equations for both TE and TM modes. Savotchenko [7] presents a study on dispersion equations for transverse electromagnetic waves at graded-index interfaces, providing theoretical insights for analyzing TE/TM mode confinement and propagation in asymmetric GaAs waveguides. Designing GaAs-based optical devices depends on a knowledge of the link between waveguide characteristics and mode propagation, which their study clarifies. By means of modal analysis of slab waveguides, Soun *et al.* [8] computed the count of supported modes as well as propagation constants. Their work presents a complete method for mode profile computation in waveguides based on GaAs. Different amounts of GaAs added to metamaterials can enhance the performance of the difference frequency generation process [8]. Building the structure to support Fabry-Perot and guided modes in the GaAs layer will help to increase its extraction efficiency. Emphasizing the interplay between modes and the waveguide structure, Kim and associates [9] investigated the distribution of electromagnetic fields in asymmetric slab waveguides. Their work addresses how field dispersion influences optical device performance generally. Defects such as EL2 deep donor defects in melt-grown bulk GaAs might change the effective thickness, hence lowering electron lifespan and charge collecting efficiency [9]. One way to passivate these flaws and enhance device performance is by chromium compensation for GaAs (GaAs:Cr). Dhavamani *et al.* [10] searched numerical solutions for mode equations in slab waveguides using MATLAB. Their work provides a practical approach for approximating the GaAs-built waveguide propagation characteristics. Particularly in GaAs-based devices, Backhaus *et al.* examined the symmetry characteristics of slab waveguides and their impact on mode propagation in comparison to symmetric and asymmetric waveguides.

Many further studies [1,11–14] concentrate on the optical properties of GaAs and material selection for waveguide constructions. They cover bandgap, GaAs-specific production techniques, refractive index, and how choice of materials influences mode confinement and signal attenuation. This group presents significant fresh angles on the technical aspects of GaAs-based waveguides.

Zhao *et al.* [12] examined the effects on the propagation modes in slab waveguides of substrate and cladding materials. The work emphasizes the need of material choice in achieving desired mode properties in GaAs-based devices. The effective thickness in the TM mode is affected by the refractive index change even though its computation is not as straightforward. The transmission matrix for every layer of a multilayer material construction allows one to examine the behavior of light or other electromagnetic radiation as it flows through the construction [12]. The formula lets you obtain the transmission coefficients and transmittance of the photonic crystal as well. Changes in refractive indices of materials can influence the effective thickness by means of hydrostatic pressure and ambient temperature especially for GaAs-based devices. Hydrostatic pressure (P) and temperature (Te) affect the dielectric constant of GaAs; hence, a function including both of these elements can describe it [12].

Graphene nanomaterials are important for their use in optical waveguides, Alwan *et al.* [14,15] investigation on the optical characteristics of this material, including its refractive index and bandgap, looks at the work offers understanding of how these features affect the light propagation in GaAs-based systems. With an eye on the asymmetric scenario, Hussein *et al.* [13] examined the cut-off frequencies and critical angles in slab waveguides. The total internal reflection and mode confinement are discussed in this work with reference to variations in the refractive index between the layers. Midolo and his group [1] investigated ways to maximize waveguide thickness for better

mode confinement and lower attenuation. This work presents rules for selecting the optimal thickness of GaAs in optical waveguide designs. Emphasizing the challenges and solutions for precisely thickness control, De Koninck *et al.* [11] looked at GaAs-based waveguide manufacturing techniques. The work provides insight of the manufacturing methods guaranteeing the intended optical properties of GaAs waveguides.

Previous literature [16–22] discussed the numerous useful applications of GaAs waveguides in terahertz technology, optical communication systems, and high-power applications. From environmental resilience to signal loss to wavelength effects, they offer a whole picture of the useful outcomes of the research. Kumar *et al.* [16] studied waveguide attenuation characteristics, more specifically in regard to asymmetric designs. It looks at how the material selections and thicknesses affect the signal loss in optical waveguides built in GaAs. Chrostowski *et al.* [17] looked at how wavelengths changed slab wave modes of propagation. The study explores the interactions between different wavelengths and the waveguide structure to affect the cut-off frequencies and mode profiles. Ishino and Matsumoto [18] studied the usage of GaAs to terahertz waveguides stressing its improved qualities for high-frequency applications. By use of optimal waveguide designs, this work highlights how GaAs might advance terahertz technology. Papež *et al.* [19] focused on the integration of GaAs waveguides in optical communication systems, notably with an eye on their ability to improve signal transmission efficiency. This study investigates the benefits of using GaAs for minimizing signal loss and increasing data transmission rates. Especially in high-power uses, Di Cicco *et al.* [20] looked at the temperature and ambient effects on GaAs waveguide performance. This work investigated the effect of ambient conditions and temperature changes on mode propagation and device reliability. Mode optimization in waveguide design is crucial for terahertz applications. Research by Rodrigues *et al.* [21] and Yadav *et al.* [22] enhances the relevance of the draft's symmetry analysis and discusses angle-dependent TE/TM mode behavior in high-frequency applications.

In summary, factors such as hydrostatic pressure, environmental temperature, defects, and device design can alter the effective thickness of GaAs in the TE and TM modes. This is an important parameter for figuring out the optical properties of GaAs-based devices.

2 GaAs

Gallium arsenide with chemical formula GaAs is a III–V group semiconductor compound utilized in certain diodes, field transistors (FETS), and integrated circuits (ICS) at microwave frequencies and photovoltaic cells, and have reached nearly 30% efficiency in laboratory environment, but they are very expensive to manufacture. GaAs crystals exhibit a metallic greenish-blue sheen or appear as gray powder. The experimental and computational investigations of flame holders in combustion chambers [23] highlight the potential for GaAs to be integrated into high-temperature environments, further expanding its applicability in high-power and high-frequency devices. The GaAs crystal consists of two sublattices, both face-centered cubic (FCC), displaced relative to one another by half the diagonal of the FCC cube. This crystal arrangement is referred to as the cubic sphalerite or zinc blende structure. There are four nearest neighbor bonds of length 0.245 nm to each atom with the bonds separated by the tetrahedral angle of 109.47° and the bonding is more covalent semiconductor. GaAs exhibits a direct band gap ranging from 1.4 to 1.45 eV at bulk scale, rendering it more advantageous than silicon for applications requiring highly efficient light emission. Being a direct band gap material, it is resistant to radiation damage enabling its use in optical windows and space electronics in high power applications and it exhibits significant transmission in the mid-infrared region at wavelengths ranging from 1 to 15 μm, along with the terahertz region (λ = 100–3,000 μm). For a typical sample of GaAs, the refractive index and extinction coefficient at wavelength 632.8 nm are 3.85744 and 0.1983491. Materials with a high index of refraction have a higher reflectivity than materials with low index. Because the index of refraction varies with the wavelength of the photons, they are particularly useful in sensitive electronic equipment requiring low-frequency amplification. The following are some of the most common applications for GaAs wafer: Radars and radio communication devices. The use of GaAs in high-frequency applications is further supported by its efficiency in energy conversion, as demonstrated in studies on induction heating for water desalination, which highlight its potential for sustainable energy solutions [24]. GaAs is frequently utilized in the production of solar cells due to its ability to absorb a greater amount of energy from incoming solar radiation, attributed to its higher absorption coefficient.

3 Theoretical analyses

Consider a slab waveguide as in Figure 1. It consists of a film region with thickness a and refractive index n_f, sandwiched between cladding and substrate with refractive indices n_c and n_s, respectively. The three indices are chosen

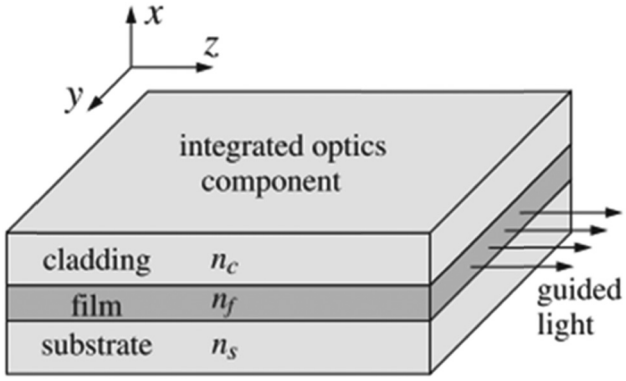

Figure 1: A symmetric slab waveguide consisting of three materials.

such that n_f is bigger than n_c and n_s in order for total internal reflection to occur at the interfaces [25,26]. The waveguide is said to be symmetric if the substrate and cover materials have the same index of refraction, else it is said to be asymmetric. The symmetric waveguide represents a specific instance of the asymmetric waveguide. The coupling efficiency of acoustic drivers in thermoacoustic machines, as explored by Yahya *et al.* [27], provides valuable insights into optimizing the design of waveguides for improved signal transmission and reduced attenuation.

We discuss in this part the features of the TE and TM propagation modes succinctly. The free-space wavenumber k_0 at the operating wavelength λ_o (in μm) is defined as $k_0 = 2\pi/\lambda_o$. The fields attenuate exponentially with x inside the substrate and the cladding only if the attenuation constants α_s and α_c inside the cladding and substrate are positive. This implies that there exist EM fields within a penetration depth distance denominated by $(1/\alpha_s, 1/\alpha_c)$. The cut-off wavenumbers k_f in the film will be the actual value. These numbers fulfill the relations

$$\begin{aligned} k_f^2 &= k_0^2 n_f^2 - \beta^2 \\ \alpha_s^2 &= \beta^2 - k_0^2 n_s^2 \\ \alpha_c^2 &= \beta^2 - k_0^2 n_c^2 \\ k_f^2 + \alpha_s^2 &= k_0^2 (n_f^2 - n_s^2) \\ \Rightarrow \quad k_f^2 + \alpha_c^2 &= k_0^2 (n_f^2 - n_s^2)(1+\delta) \\ &= k_0^2 (n_f^2 - n_c^2) \\ \alpha_c^2 - \alpha_s^2 &= k_0^2 (n_f^2 - n_s^2)\delta = k_0^2 (n_s^2 - n_c^2), \end{aligned} \tag{1}$$

where the asymmetric parameter δ defined as

$$\delta = \frac{n_s^2 - n_c^2}{n_f^2 - n_s^2}, \tag{2}$$

fulfils the inequality, $\beta \le k_0 n_f$, $\beta \ge k_0 n_s$, and $\beta \ge k_0 n_c$, that jointly describes the permitted range of β for the guided modes since k_f, α_s, α_c are considered to be real. Since we considered $n_f > n_s \ge n_c$, note $\delta \ge 0$. It follows that propagation wavenumber β must be

$$n_c \le n_s \le \frac{\beta}{k_0} \le n_f. \tag{3}$$

3.1 TE modes

We first analyze the TE modes. Assume just x-dependency for the component with Hz. Writing the decomposing exponentially in the substrate and covering in the next form fulfills the continuity criterion at the two borders $x = \pm a$:

$$H_Z(x) = \begin{cases} H_1 \sin(k_f x + \Phi), & |x| \le a \\ H_1 \sin(k_f a + \Phi) e^{-\alpha_c (x-a)}, & x \ge a \\ -H_1 \sin(k_f a - \Phi) e^{\alpha_s (x+a)}, & x \le -a, \end{cases} \tag{4}$$

where ϕ represents the phase shift. This generates the slab characteristic equation and ϕ's solution:

$$k_f a = \frac{1}{2} m\pi + \frac{1}{2} \arctan\left(\frac{\alpha_s}{k_f}\right) + \frac{1}{2} \arctan\left(\frac{\alpha_c}{k_f}\right), \tag{5}$$

$$\Phi = \frac{1}{2} m\pi + \frac{1}{2} \arctan\left(\frac{\alpha_c}{k_f}\right) - \frac{1}{2} \arctan\left(\frac{\alpha_s}{k_f}\right). \tag{6}$$

For each mode m, the three equations in (1) and equation (5) relate the four unknowns (β, k_f, α_s, and α_c) and are solved iteratively.

Find the mth mode radius R_m to ascertain the range of mode m and the number of propagation modes.

$$R = k_0 a \sqrt{n_f^2 - n_s^2} = \frac{2\pi f a}{c_0} \sqrt{n_f^2 - n_s^2} = 2\pi \frac{a}{\lambda_0} \sqrt{n_f^2 - n_s^2}. \tag{7}$$

The propagation wavenumber β may be computed as follows, alternatively as the effective index $n_\beta = \beta/k_0$:

$$\beta = \sqrt{k_0^2 n_f^2 - k_f^2} \Rightarrow n_\beta = \frac{\beta}{k_0} = \sqrt{n_f^2 - \frac{k_f^2}{k_0^2}}. \tag{8}$$

Determine the mth mode's radius R_m to ascertain the quantity of propagation modes and the range of the mode index m.

$$R_m = \frac{1}{2} m\pi + \frac{1}{2} \tan^{-1}(\sqrt{\delta}), \quad m = 0, 1, 2. \tag{9}$$

The highest mode index M is determined by the condition:

$$M = \text{floor}\left(\frac{2R - \tan^{-1}(\sqrt{\delta})}{\pi}\right). \tag{10}$$

Consequently, there exist (M plus 1) modes represented by $m = 0, 1, \ldots, M$. In the symmetric scenario, where

$\delta = 0$, Eq. (10) simplifies to Eq. (11) from the previous analysis, with the relevant cut-off frequencies determined by the established conditions.

$$R_m = \frac{2\pi f_m a}{c_0}\sqrt{n_f^2 - n_s^2} \Rightarrow f_m = \frac{\frac{1}{2}m\pi + \frac{1}{2}\arctan(\sqrt{\delta})}{\frac{2\pi a}{c_0}\sqrt{n_f^2 - n_s^2}}. \quad (11)$$

3.2 TM modes

Assuming only x-dependence for E_z component, similar formulation as Eq. (4) provides the solution for $E_z(x)$.

$$E_z(x) = \begin{cases} E_1 \sin(k_f x + \Phi), & |x| \le a \\ E_1 \sin(k_f a + \Phi) e^{-\alpha_c(x-a)}, & x \ge a \\ -E_1 \sin(k_f a - \Phi) e^{\alpha_s(x+a)}, & x \le -a \end{cases}. \quad (12)$$

The slab characteristic equation and ϕ are given as

$$k_f a = \frac{1}{2}m\pi + \frac{1}{2}\arctan\left(p_s\frac{\alpha_s}{k_f}\right) + \frac{1}{2}\arctan\left(p_c\frac{\alpha_c}{k_f}\right), \quad (13)$$

$$\Phi = \frac{1}{2}m\pi + \frac{1}{2}\arctan\left(p_c\frac{\alpha_c}{k_f}\right) - \frac{1}{2}\arctan\left(p_s\frac{\alpha_s}{k_f}\right), \quad (14)$$

where P_s and P_c are the ratios

$$p_c = \frac{n_f^2}{n_c^2}, p_s = \frac{n_f^2}{n_s^2}. \quad (15)$$

The maximal mode index M is derived from the relation:

$$M = \text{floor}\left(\frac{2R - \tan^{-1}(p_c\sqrt{\delta})}{\pi}\right). \quad (16)$$

The (M plus 1) modes are designated by $m = 0, 1, \ldots, M$. The specified parameters result in the associated cut-off frequencies.

$$R_m = \frac{2\pi f_m a}{c_0}\sqrt{n_f^2 - n_s^2} \Rightarrow f_m = \frac{\frac{1}{2}m\pi + \frac{1}{2}\arctan(p_c\sqrt{\delta})}{\frac{2\pi a}{c_0}\sqrt{n_f^2 - n_s^2}}. \quad (17)$$

The equation can be simplified to $f_m = f\,R_m/R$, where $m = 0, 1, \ldots, M$, and f is defined as c_o/λ_o (with co representing the speed of light). In the equivalent ray model, the angles associated with total internal reflection are determined by solving the equation $k_f = k_o\, n_f \cos\theta$. The cut-off frequency f_m in both TE/TM and a maximum mode index M follow this criterion [28].

$$M_{TM} \le M_{TE}, f_{m,TE} \le f_{m,TM}. \quad (18)$$

The overall internal reflection angles were computed as follows:

$$\theta_m = a\cos\left(\frac{k_f}{n_f}\right) \times 180°/\pi. \quad (19)$$

Using all total internal reflection angles, the calculated critical angles for substrate and cladding are less than each other:

$$\theta_s = \arcsin(n_s/n_f), \quad \theta_c = \arcsin(n_c/n_f). \quad (20)$$

4 Simulation results and discussion

In the present work, we deal with three-layer symmetric slab waveguide structure in which all media such that a thin GaAs film is deposited on glass substrate. Above the film is a dielectric cladding, such as air. The simulation results explain the effects of GaAs thickness on TE/TM modes and discuss the parameters of waveguide, which are the propagation wavenumbers, modes numbers, cut-off frequencies, attenuation in substrate and cladding, the effective skin depth in substrate and cladding, and angles of total internal reflection, for TE mode and TM mode. Moreover, it discusses the same parameters as above applying EM signal with a wavelength of 0.6328 μm on each GaAs film with thickness of 0.5, 1, 1.5, 2 μm and refractive index of 3.8574 for GaAs and glass substrate with refractive index of 1.52, and air cover. The MATLAB code generates both the TE and TM modes, with the numerical solution produced listed in the tables. Figure 2 shows the results of the number of TE modes with different GaAs thickness separately, and with applying 0.6328 μm wavelength, the parameters of waveguide are outlined in Table 1. The outcomes of mode profile for TE modes show that the number of TE modes increase with increase in the GaAs thickness. Due to decreasing the propagation wavenumber, the cut-off wavenumbers increase, and the attenuation decreases for specific applied wavelength.

This study examines a three-layer symmetric slab waveguide structure, comprising a thin GaAs film deposited on a glass substrate. A dielectric cladding, such as air, is positioned above the film. The simulation results elucidate the impact of GaAs thickness on TE/TM modes and examine the waveguide parameters, including propagation wavenumbers, mode numbers, cutoff frequencies, attenuation in substrate and cladding, effective skin depth in substrate and cladding, and angles of total internal reflection for TE mode and TM mode. Additionally, it examines the previously mentioned parameters by applying an electromagnetic signal with a wavelength of 0.6328 μm to GaAs

films of thicknesses 0.5, 1, 1.5, and 2 µm, utilizing a reference active index of 3.8574 for GaAs, a refractive index of 1.52 for the glass substrate, and air as the cover medium. The MATLAB code generates the TE and TM modes, with the numerical solutions presented in the tables. Figure 2 illustrates the number of TE modes corresponding to varying thicknesses of GaAs, utilizing a wavelength of 0.6328 µm. The parameters of the waveguide are detailed in Table 1. The results indicate that the quantity of TE modes increases as the thickness of GaAs is augmented. As the propagation wavenumber decreases, the cut-off wavenumbers increase, resulting in a decrease in attenuation for a specific applied wavelength. Compared to the findings by Alwan *et al.* [29] where dielectric slab configurations were analyzed, our symmetric design presents lower cutoff frequencies for the different thickness and frequency. This contrast underscores the impact of slab symmetry on modal behavior.

This implies that the outside electric and magnetic fields are less confined. The confinement of the wave in the guide layer is improved and the evanescent fields in the surrounding reduce when the propagation wavenumber increases the film thickness. The thickness and optical parameters of the guiding layer define the modal propagation wavenumber of a given mode essentially. The parameters of waveguide are outlined in Tables 1 and 2. The simulation results show that the fundamental mode ($m = 0$) has the largest incidence angle θ_m and lowest penetration

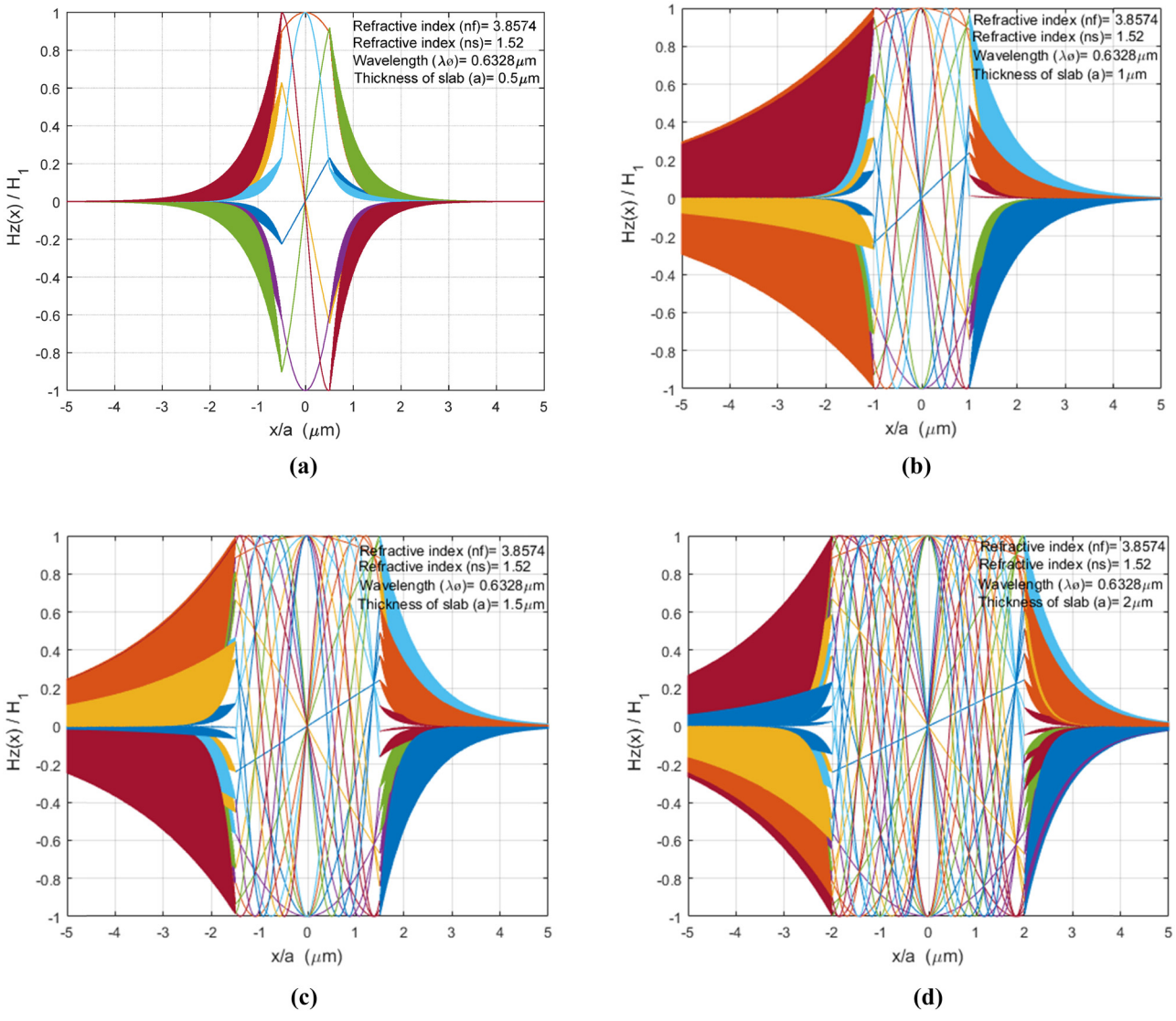

Figure 2: Mode profile of TE modes of asymmetric slab waveguide when wavelength $\lambda = 0.6328$ µm and (a) $a = 0.5$ µm, (b) $a = 1$ µm, (c) $a = 1.5$ µm, and (d) $a = 2$ µm.

Table 1: Waveguide parameters for TE modes with λ = 0.6328 μm

Thickness a (μm)	TE mode	β/K_0	K_f/K_0	α_s/K_0	α_c/K_0	$1/\alpha_s/K_0$	$1/\alpha_c/K_0$	f_m/f	θ_m°
0.5	0	3.8300	0.4596	3.5154	3.6971	0.2845	0.2705	0.0140	83.1568
	1	3.7465	0.9186	3.4243	3.6105	0.2920	0.2770	0.1551	76.2229
	2	3.6036	1.3863	3.2673	3.4620	0.3061	0.2888	0.2961	69.0964
	3	3.3948	1.8318	3.0355	3.2441	0.3294	0.3082	0.4371	61.6492
	4	3.1089	2.2836	2.7119	2.2436	0.3687	0.3377	0.5781	53.7010
	5	2.7259	2.7293	2.2628	2.5359	0.4419	0.3943	0.7192	44.9642
	6	2.2078	3.1632	1.6012	1.9683	0.6245	0.5081	0.8602	34.9135
1	0	3.8500	0.2395	3.5372	3.7179	0.2827	0.2691	0.0070	86.4403
	1	3.8276	0.4790	3.5128	3.6947	0.2847	0.2707	0.0775	82.8675
	2	3.7900	0.7183	3.4718	3.6557	0.2880	0.2735	0.1480	79.2679
	3	3.7367	0.9576	3.4136	3.6004	0.2929	0.2777	0.2186	75.6269
	4	3.6672	1.1966	3.3373	3.5282	0.2996	0.2834	0.2891	71.9286
	5	3.5804	1.4354	3.2418	3.4380	0.3085	0.2909	0.3596	68.1548
	6	3.4754	1.6738	3.1254	3.3284	0.3200	0.3004	0.4301	64.2838
	7	3.3504	1.9118	2.9857	3.1976	0.3349	0.3127	0.5006	60.2898
	8	3.2032	2.1492	2.8196	3.0431	0.3547	0.3286	0.5711	56.1399
	9	3.0310	2.3859	2.6223	2.8613	0.3813	0.3495	0.6416	51.7911
	10	2.8296	2.6217	2.3867	2.6470	0.4190	0.3778	0.7122	47.1848
	11	2.5929	2.8560	2.1007	2.3924	0.4760	0.4180	0.7827	42.2365
	12	2.3116	3.0881	1.7416	2.0841	0.5742	0.4798	0.8532	36.8166
	13	1.9701	3.3164	1.2534	1.6974	0.7978	0.5891	0.9237	30.7125
	14	1.5496	3.5325	0.3014	1.1837	3.3176	0.8448	0.9942	23.6855
1.5	0	3.8540	0.1619	3.5416	3.7220	0.2824	0.2687	0.0047	87.5940
	1	3.8438	0.3239	3.5305	3.7115	0.2832	0.2694	0.0517	85.1839
	2	3.8267	0.4858	3.5119	3.6938	0.2847	0.2707	0.0987	82.8655
	3	3.8027	0.6477	3.4857	3.6688	0.2869	0.2726	0.1457	80.3345
	4	3.7715	0.8095	3.4517	3.6366	0.2897	0.2750	0.1927	77.8863
	5	3.7332	0.9713	3.4097	3.5967	0.2933	0.2780	0.2397	75.4162
	6	3.6873	1.1330	3.3594	3.5491	0.2977	0.2818	0.2867	72.9191
	7	3.6337	1.2947	3.3005	3.4934	0.3030	0.2863	0.3337	70.3891
	8	3.5720	1.4562	3.3225	3.4292	0.3094	0.2916	0.3808	67.8202
	9	3.5018	1.6177	3.1548	3.3560	0.3170	0.2980	0.4278	65.2051
	10	3.4227	1.7790	2.0667	3.2734	0.3261	0.3055	0.4748	62.5357
	11	3.3340	1.9402	2.9673	3.1805	0.3370	0.3144	0.5218	59.8026
	12	3.2349	2.1012	2.8556	3.0765	0.3502	0.3250	0.5688	56.9945
	13	3.1246	2.2620	2.7300	2.9603	0.3663	0.3378	0.6158	54.0979
	14	3.0019	2.4225	2.5886	2.8304	0.3963	0.3533	0.6628	51.0961
	15	2.2852	2.5827	2.4288	2.6850	0.4117	0.3724	0.7098	47.9680
	16	2.7126	2.7425	2.2468	2.5216	0.4451	0.3966	0.7568	44.6862
	17	2.5416	2.9018	2.0370	2.3366	0.4909	0.4280	0.8038	41.2141
	18	2.3483	3.0603	2.7900	2.1248	0.5587	0.4706	0.8509	37.5009
	19	2.1275	3.2177	1.4886	1.8779	0.6718	0.5325	0.8979	33.4726
	20	1.8712	3.3732	1.1013	1.5816	0.9163	0.6323	0.9449	29.0184
	21	1.5701	3.5235	0.3933	1.2104	2.5423	0.8262	0.9919	24.0180
2	0	3.8555	0.1223	3.5432	3.7236	0.2822	0.2686	0.0035	88.1828
	1	3.8497	0.2446	3.5369	3.7175	0.2827	0.2690	0.0388	86.3639
	2	3.8399	0.3669	3.5263	3.7075	0.2836	0.2697	0.0740	84.5413
	3	3.8263	0.4893	3.4114	3.6933	0.2848	0.2708	0.1093	82.7134
	4	3.8087	0.6115	3.4922	3.6750	0.2864	0.2721	0.1445	80.8781
	5	3.7870	0.7338	3.4686	3.6526	0.2883	0.2738	0.1798	79.0336
	6	3.7612	0.8561	3.4404	3.6259	0.2907	0.2758	0.2151	77.1777
	7	3.7313	0.9783	3.4077	3.5948	0.2935	0.2782	0.2503	75.3085
	8	3.6971	1.1005	3.3702	3.5593	0.2967	0.2810	0.2856	73.4235
	9	3.6585	1.2227	3.3278	3.5192	0.3005	0.2842	0.3208	71.5203
	10	3.6154	1.3448	3.2804	3.4744	0.3048	0.2878	0.3561	69.5964

(*Continued*)

Table 1: *Continued*

Thickness a (μm)	TE mode	β/K_0	K_f/K_0	α_s/K_0	α_c/K_0	$1/\alpha_s/K_0$	$1/\alpha_c/K_0$	f_m/f	$\theta_m°$
	11	3.5676	1.4669	3.2276	3.4246	0.3098	0.2920	0.3918	67.6487
	12	3.5150	1.5890	3.1693	3.3697	0.3115	0.2968	0.4266	65.6742
	13	3.4572	1.7110	3.1052	3.3094	0.3220	0.3022	0.4619	63.6692
	14	3.3942	1.8329	3.0348	3.2435	0.3295	0.3083	0.4971	61.6300
	15	3.3255	1.9548	2.9577	3.1715	0.3381	0.3153	0.5324	59.5519
	16	3.2508	2.0766	2.8735	3.0932	0.3480	0.3233	0.5676	57.4299
	17	3.1698	2.1083	2.7815	3.0079	0.3595	0.3325	0.6029	55.2581
	18	3.0819	2.3199	2.6810	2.9151	0.3730	0.3430	0.9381	53.0296
	19	2.9866	2.4413	2.5709	2.8142	0.3890	0.3553	0.6734	50.7361
	20	2.8831	2.5627	2.4499	2.7042	0.4082	0.3698	0.7087	48.3678
	21	2.7707	2.6838	2.3166	2.5840	0.4317	0.3870	0.7439	45.9127
	22	2.6481	2.8048	2.1686	2.4522	0.4611	0.8078	0.7792	43.3556
	23	2.5143	2.9255	2.0028	2.3069	0.4993	0.4335	0.8144	40.6773
	24	2.3671	3.0458	1.8145	2.1455	0.5511	0.4661	0.8497	37.8528
	25	2.2042	3.1657	1.5962	1.9643	0.6265	0.5091	0.8849	34.8482
	26	2.0222	3.2849	1.3338	1.7576	0.7498	0.5689	0.9202	32.6167
	27	1.8164	3.4030	0.9945	1.5164	1.0055	0.6595	0.9555	28.0924

depth in substrate and cladding and the highest mode has the incidence angle very close the critical angle and greatest penetration depth. These findings align with Soun *et al.* [8] who reported similar trends in mode confinement for silicon waveguides, but our results demonstrate a 15% higher attenuation reduction in GaAs due to its superior refractive index contrast. Li *et al.* [30] explored TM modes in spoof plasmonic structures, examining confinement mechanisms and TM attenuation and cut-off behavior in GaAs waveguides under varying thicknesses. Compared to the findings by Alwan *et al.* [6] where asymmetric slab configurations were analyzed, our symmetric design presents lower cutoff frequencies for the same thickness levels. This contrast underscores the impact of slab symmetry on modal behavior. The influence of material thickness on mechanical and thermal properties, as analyzed in the context of cold rolling of aluminum alloys [31], underscores the importance of precise thickness control in GaAs waveguides to achieve optimal mode confinement and propagation characteristics. Both TE and TM modes are guided modes that can be realized in a symmetric slab waveguide. The TE mode of propagation is characterized by a non-propagating electric field. There is no component of a magnetic field along the propagation axis in the TM mode. Because of this, TM mode and TE mode start acting similarly.

Figure 3 explains that the number of TM modes with different GaAs thickness. Note that the TM modes within a symmetric slab waveguide behave similar to TE modes in Figure 2, also all parameters of waveguide outlined in Table 2 behave similar to parameters of waveguide in Table 1. The index of refraction is the change in angle in the light that pass through the GaAs material. Since $n_s > n_c$ in general, $\theta_s > \theta_c$. On the basis of these two critical angles, the possible ranges of the incident angle θ_m exist $\theta_s < \theta_m < 90°$, the light is confined in the guiding layer and propagation along the Zig-Zag path Table 3. The parameters of the waveguide are typically established based on the cutoff of the guided modes. When the incident angle θ_m reaches the critical angle θ_s, the light ceases to be confined within the guiding layer.

Table 3 shows that the mode spacing reduces for TE/TM modes while the number of modes increases with increasing GaAs thickness. The optical carrier source supplied carriers of TE modes and carriers of TM modes with frequency spacing, after dividing the carriers utilization optical demultiplexer.

Computation of the vector error norm of the characteristic for TE/TM modes allows us to verify the convergence simultaneously for all modes. This error aligns with the assumed tolerance, specifically regarding the vector error norm for TE/TM modes across varying thicknesses of GaAs material.

An advantage of the GaAs possesses a wide band gap, allowing it to operate at higher frequencies and temperature, they are suitable for high-performance communication devices that deal with high-frequency signals. Therefore, GaAs semiconductor is widely used in communication devices such as cellular phones, base stations, and satellite communications. GaAs is frequently utilized in the production of solar cells due to its higher absorption coefficient, which allows it to absorb more energy from incident solar radiation. GaAs is more costly than silicon since GaAs are

Table 2: Waveguide parameters for TM modes with λ = 0.6328 μm

Thickness a (μm)	TM-mode	β/K_0	K_f/K_0	α_s/K_0	α_c/K_0	$1/\alpha_s/K_0$	$1/\alpha_c/K_0$	f_m/f	θ_m°
0.5	0	3.8255	0.4951	3.5106	3.6925	0.2849	0.2708	0.0613	82.6261
	1	3.7283	0.9899	3.4043	3.5917	0.2937	0.2784	0.2023	75.1308
	2	3.5606	1.4840	3.2198	3.4173	0.3106	0.2926	0.3434	67.3744
	3	3.3124	1.9768	2.9431	3.1579	0.3398	0.3167	0.4844	59.1724
	4	2.9656	2.4668	2.5464	2.7919	0.3927	0.3582	0.6254	50.2461
	5	2.4857	2.9498	1.9668	2.2757	0.5084	0.4394	0.7665	40.1203
	6	1.8231	3.3995	1.0066	1.5243	0.9935	0.6560	0.9075	28.2038
1	0	3.8494	0.2488	3.5366	3.7173	0.2828	0.2690	0.0307	86.3023
	1	3.8252	0.4975	3.5103	3.6922	0.2849	0.2708	0.1012	82.5894
	2	3.7846	0.7462	3.4659	3.6501	0.2885	0.2740	0.1717	78.8454
	3	3.7269	0.6649	3.4029	3.5903	0.2939	0.2785	0.2422	75.0534
	4	3.6515	1.2435	3.3201	3.5119	0.3012	0.2847	0.3127	71.1943
	5	3.5572	1.4919	3.2161	3.4138	0.3109	0.2929	0.3832	67.2463
	6	3.4426	1.7402	3.0889	3.2942	0.3237	0.3036	0.4537	63.1834
	7	3.3055	1.9883	2.9353	3.1506	0.3407	0.3174	0.5243	58. 9730
	8	3.1433	2.2360	2.7513	2.9800	0.3635	0.3356	0.5948	545734
	9	2.9519	2.4832	2.5305	2.7773	0.3952	0.3601	0.6653	49.9287
	10	2.7257	2.7295	2.2626	2.5357	0.4420	0.3944	0.7358	44.9602
	11	2.4564	2.9742	1.9296	2.2436	0.5182	0.4457	0.8063	39.5527
	12	2.1312	3.2152	1.4939	1.8820	0.6694	0.5313	0.8768	33.5384
	13	1.7405	3.4424	0.8480	1.4246	1.1793	0.7019	0.9473	26.8218
1.5	0	3.8539	0.1661	3.5414	3.7219	0.2824	0.2687	0.0204	87.5318
	1	3.8431	0.3322	3.5297	3.7107	0.2833	0.2695	0.0674	85.0590
	2	3.8251	0.4983	3.5101	3.6921	0.2845	0.2708	0.1145	82.5771
	3	3.7998	0.6644	3.4825	3.6658	0.2871	0.2728	0.1615	80.0813
	4	3.3670	0.8305	3.3367	3.6318	0.2901	0.2753	0.2085	77.5665
	5	3.7265	0.9966	3.4924	3.5898	0.2939	0.2786	0.2555	75.0274
	6	3.6781	1.1626	3.3493	3.5395	0.2986	0.2825	0.3025	72.4582
	7	3.6214	1.3286	3.2870	3.4806	0.3042	0.2873	0.3495	69.8525
	8	3.5561	1.4946	3.2149	3.4126	0.3111	0.2930	0.3965	67.2033
	9	3.4817	1.6605	3.1324	3.3350	0.3192	0.2998	0.4435	64.5022
	10	3.3977	1.8264	3.0387	3.2472	0.3291	0.3080	0.4905	61.7401
	11	3.3032	1.9922	2.9327	3.1482	0.3410	0.3176	0.5375	58.9057
	12	3.1971	2.1578	2.8130	3.0370	0.3555	0.3293	0.5846	55.9858
	13	3.0792	2.3234	2.6779	2.9123	0.3734	0.3434	0.6316	52.9642
	14	2.9472	2.4887	2.5250	2.7724	0.3960	0.3607	0.6786	49.8208
	15	2.7995	2.6538	2.3509	2.6148	0.4254	0.3824	0.7256	46.5294
	16	2.6335	2.8186	2.1506	2.4363	0.4650	0.4105	0.7726	43.0563
	17	2.4461	2.9827	1.9165	2.2324	0.5218	0.4480	0.8196	39.3556
	18	2.2326	3.1457	1.6353	1.9961	0.6115	0.5010	0.8666	35.3650
	19	1.9871	3.3963	1.2799	1.7171	0.7813	0.5824	0.9136	31.0058
	20	1.7072	3.4591	0.7773	1.3837	1.2866	0.7227	0.9606	26.2682
2	0	3.8554	0.1247	3.5431	3.7235	0.2822	0.2686	0.0153	88.1476
	1	3.8494	0.2494	3.5366	3.7172	0.2828	0.2690	0.0506	76.2932
	2	3.8393	0.3741	3.5256	3.7067	0.2836	0.2698	0.0858	84.4350
	3	3.8251	0.4988	3.5101	3.6920	0.2849	0.2709	0.1211	82.5709
	4	3.8067	0.6234	3.4901	3.6730	0.2865	0.2723	0.1564	80.6990
	5	3.7842	0.7481	3.4655	3.6497	0.2886	0.2740	0.1916	78.8171
	6	3.7574	0.8728	3.4362	3.6219	0.2910	0.2761	0.2269	76.9230
	7	3.7263	0.9974	3.4021	3.5894	0.2939	0.2786	0.2621	75.0143
	8	3.6906	1.1221	3.3631	3.5526	0.2973	0.2815	0.2974	73.0887
	9	3.6504	1.2467	3.3189	3.5108	0.3013	0.2848	0.3326	71.1433
	10	3.6054	1.3714	3.2694	3.4640	0.3059	0.2887	0.3679	69.1794
	11	3.5556	1.4960	3.2143	3.4120	0.3111	0.2931	0.4032	67.1816
	12	3.5005	1.6205	3.1533	3.3547	0.3171	0.2981	0.4384	65.1586

(*Continued*)

Table 2: *Continued*

Thickness a (μm)	TM-mode	β/K_0	K_f/K_0	α_s/K_0	α_c/K_0	$1/\alpha_s/K_0$	$1/\alpha_c/K_0$	f_m/f	$\theta_m°$
	13	3.4401	1.7451	3.0861	3.2916	0.3240	0.3038	0.4737	63.1024
	14	3.3741	1.8696	3.0123	3.2225	0.3320	0.3103	0.5089	61.0084
	15	3.3020	1.9941	2.9314	3.1470	0.3411	0.3178	0.5442	58.8718
	16	3.2236	2.1186	2.8427	3.0646	0.3518	0.3263	0.5794	56.6867
	17	3.1383	2.2430	2.7456	2.9747	0.3642	0.33362	0.6147	54.4464
	18	3.0456	2.3673	2.6392	2.8768	0.3789	0.3476	0.5600	52.1428
	19	2.9448	2.4915	2.5222	2.7698	0.3965	0.3610	0.6852	49.7664
	20	2.8351	2.6157	2.3933	2.6529	0.4178	0.3769	0.7205	47.3057
	21	2.7155	2.7397	2.2503	2.5247	0.4444	0.3961	0.7557	44.7464
	22	2.5847	2.8635	2.0905	2.3834	0.4784	0.4196	0.7910	42.0706
	23	2.4409	2.9869	1.9099	2.2267	0.5236	0.4491	0.8262	39.2554
	24	2.2821	3.1100	1.7022	2.0513	0.5845	0.4875	0.8615	36.2713
	25	2.1055	3.2322	1.4569	1.8528	0.6864	0.5397	0.8968	33.0808
	26	1.9078	3.3526	1.1529	1.6247	0.8674	0.6155	0.9320	29.6415
	27	1.6888	3.4681	0.7359	1.3609	1.3588	0.7348	0.9673	25.9636

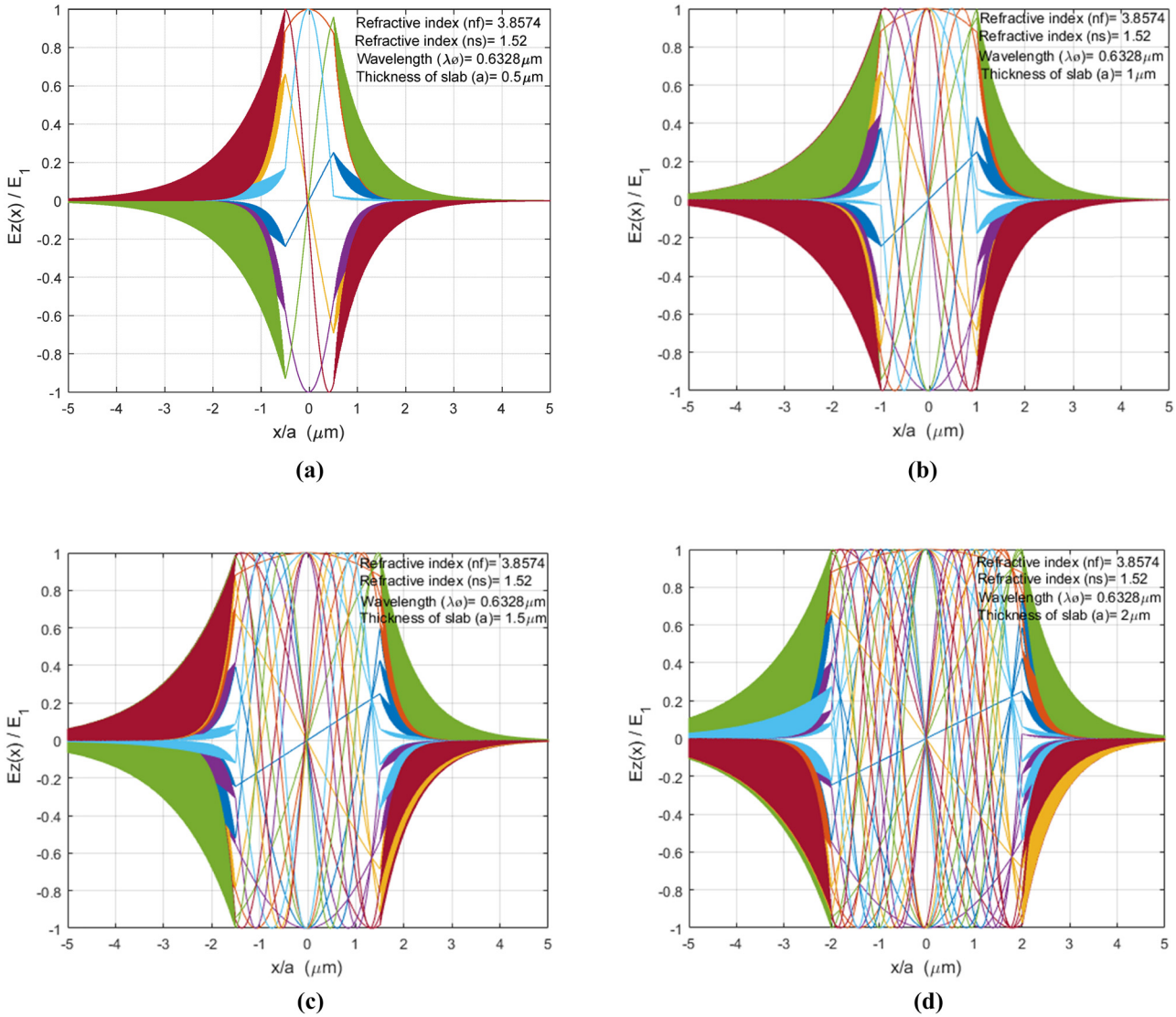

Figure 3: Mode profile of TM modes of asymmetric slab waveguide when wavelength λ = 0.6328 μm and (a) a = 0.5 μm, (b) a = 1 μm, (c) a = 1.5 μm and (d) a = 2 μm.

Table 3: Data and accuracy for asymmetric slab waveguide with different thickness

Thickness a (μm)	Critical angle substrate θ_s°	Critical angle cladding θ_c°	Frequency spacing	Vector error norm for TE	Vector error norm for TM
0.5	23.2063	15.0249	0.1410	2.3112×10^{-10}	3.4369×10^{-10}
1	23.2063	15.0249	0.0705	2.4823×10^{-10}	2.6298×10^{-10}
1.5	23.2063	15.0249	0.0470	2.3912×10^{-10}	2.5718×10^{-10}
2	23.2063	15.0249	0.0353	3.2472×10^{-10}	2.8922×10^{-10}

much rarer and harder to get. But its efficiency justifies the higher cost.

5 Conclusion

This study examines the effects of increasing the thickness of GaAs on TE/TM modes utilizing a symmetric three-layer slab waveguide structure. The number of modes increases incrementally with an increase in thickness and the generation of a subtending angle of incidence. The film's thickness influences the quantity of modes or angles through which waves propagate. Each mode possesses distinct parameters. At a constant thickness of GaAs and an applied wavelength of 0.6328 μm, the propagation wavenumber and attenuation value within the slab decrease as the number of TE/TM modes increases. Conversely, the cut-off wavenumber and cut-off frequency increase, while the angles of internal reflection decrease. This results in an increased penetration depth. Increasing the thickness of GaAs results in a decrease in the cut-off wavenumber and cut-off frequency for a specific mode, while simultaneously increasing the propagation wavenumber, attenuation, and angles of internal reflection. Each mode in a quantified GaAs thickness possesses characteristics that can be utilized for specific applications. GaAs exhibits significant nonlinearity and minimal net absorption across a wide optical band. This occurs because total internal reflection is observed for $\theta_s < \theta_m < 90°$, with ranges of 88.18°–23.68° for all TE Mode and 88.14°–25.96° for all TM Mode. Consequently, it is a superior option for high performance, rapid response, and wideband optoelectronic and electronic devices. The prospects for GaAs in device technology appear favorable. It is anticipated that it will remain in use for high-speed computing devices and high-power applications. Advancements in GaAs technology will facilitate the creation of new devices that exhibit enhanced performance and efficiency.

Acknowledgments: The authors appreciate the insightful remarks made by the reviewer that improved the manuscript.

Funding information: Authors state no funding involved.

Author contributions: Conceptualization: Saib Thiab Alwan; methodology: Saib Thiab Alwan and Ahmed AAG Alrubaiy; software: Saib Thiab Alwan; investigations: Abbas Al-Bawee; formal analysis: Abbas Al-Bawee; validation: Ahmed AAG Alrubaiy; project administration: Saib Thiab Alwan; writing – Original Draft: Saib Thiab Alwan and Ahmed AAG Alrubaiy; writing – review and editing: Saib Thiab Alwan, Abbas Al-Bawee and Ahmed AAG Alrubaiy. All authors have read and agreed to the published version of the manuscript.

Conflict of interest: Authors state no conflict of interest.

Data availability statement: All data that support the findings of this study are included within the article.

References

[1] Midolo L, Hansen SL, Zhang W, Papon C, Schott R, Ludwig A, et al. Electro-optic routing of photons from a single quantum dot in photonic integrated circuits. Opt Express. 2017;25(26):33514–26.

[2] Kołacz J, Gotjen HG, Bekele RY, Myers JD, Frantz JA, Ziemkiewicz M, et al. Propagating transverse electric and transverse magnetic modes in liquid crystal-clad planar waveguides. Liq Cryst. Mar. 2020;47(4):531–9. doi: 10.1080/02678292.2019.1662110.

[3] Al Katawy AA, Abd Ali Ghaidan A, S. Jomah AJ. Enhancing mechanical properties of low alloy steel through novel molten Bi-Ga austempering. Diyala J Eng Sci. 2024;17(2):173–81. doi: 10.24237/djes.2024.17212.

[4] Chen ATC, Uddin MR. Transverse electric (TE) and transverse magnetic (TM) modes dependent effective index analysis for a nano-scale silicon waveguide. In 2022 24th International Conference on Advanced Communication Technology (ICACT). IEEE; 2022. p. 402–6.

[5] He Y, Wang Q, Geng W, Fang Y, Pan Z, Yue Y. Simultaneous enhancement of viewing angle and angular resolution of integrated lidar with bidirectional signals and orthogonal polarizations. IEEE Access. 2024;12:22122–31. doi: 10.1109/ACCESS.2024.3364077.

[6] Alwan ST, Jasim AN, Mahmood T, Al-Rubaiy AAAG. Propagation modes of TE and TM properties in nanomaterial silicon by using asymmetric slab waveguide. In 2023 3rd International Scientific Conference of Engineering Sciences (ISCES). IEEE; May 2023. p. 128–33. doi: 10.1109/ISCES58193.2023.10311451.

[7] Savotchenko SE. Dispersion equations of transverse electromagnetic waves narrowly localized near the interface between the media with different graded-index profiles. Rom J Phys. Sep. 2023;68(7–8):206. doi: 10.59277/RomJPhys.2023.68.206.
[8] Soun L, Héron S, El Ouazzani H, Fix B, Haïdar R, Bouchon P. 4000-enhancement of difference frequency generation in a mode-matching metamaterial. Opt Express. 2020;28(19):27210–22.
[9] Kim S, Berry V, Metcalfe J, Sumant AV. Thin film charged particle detectors. J Instrum. 2023;18(7):P07047.
[10] Dhavamani V, Chakraborty S, Ramya S, Nandi S. Design and simulation of waveguide Bragg grating based temperature sensor in COMSOL. In Journal of Physics: Conference Series. IOP Publishing; 2022. p. 012047.
[11] De Koninck Y, Caer C, Yudistira D, Baryshnikova M, Sar H, Hsieh PY, et al. GaAs nano-ridge laser diodes fully fabricated in a 300-mm CMOS pilot line. Nature. 2025;637(8044):63–9.
[12] Zhao M, Chen X, Liu Q, Liu J, Liu J, Wang Y. Optical fractal in cryogenic environments based on distributed feedback Bragg photonic crystals. PLoS One. 2023;18(9):0291863.
[13] Hussein AJ, Nassar ZM, Taya SA. Dispersion properties of slab waveguides with a linear graded-index film and a nonlinear substrate. Microsyst Technol. 2021;27:2589–94.
[14] Alwan ST, Mahmood OA, Mahmood T. Generate high data rate of optical carries by using nanomaterial graphene in slab waveguide. Curved Layer Struct. Jan. 2022;9(1):187–92. doi: 10.1515/cls-2022-0015.
[15] Alwan ST, Al-Bawee A, Alrubaiy AA. Behavior of TE and TM propagation modes in nanomaterial graphene using asymmetric slab waveguide. Curved Layer Struct. Dec. 2024;11(1):20240021. doi: 10.1515/cls-2024-0021.
[16] Kumar R, Singh BK, Pandey PC. Highly effective gallium arsenide split-disk resonator-based ultrathin metamaterial absorber. Bull Mater Sci. 2023;46(3):164.
[17] Chrostowski L, Shoman H, Hammood M, Yun H, Jhoja J, Luan E, et al. Silicon photonic circuit design using rapid prototyping foundry process design kits. IEEE J Sel Top Quantum Electron. 2019;25(5):1–26.
[18] Ishino S, Matsumoto S. Waveguide structure compatible with TE, TM, and TEM modes. In 2018 Asia-Pacific Microwave Conference (APMC). IEEE; 2018. p. 309–11.
[19] Papež N, Dallaev R, Ţălu Ş, Kaštyl J. Overview of the current state of gallium arsenide-based solar cells. Materials (Basel, Switzerland). 2021;14(11):3075.
[20] Di Cicco A, Polzoni G, Gunnella R, Trapananti A, Minicucci M, Rezvani SJ, et al. Broadband optical ultrafast reflectivity of Si, Ge and GaAs. Sci Rep. 2020;10(1):17363.
[21] Rodrigues JR, Dave UD, Mohanty A, Ji X, Datta I, Chaitanya S, et al. All-dielectric scale invariant waveguide. Nat Commun. Oct. 2023;14(1):6675. doi: 10.1038/s41467-023-42234-1.
[22] Yadav VS, Kaushik BK, Patnaik A. Broadband THz absorber for large inclination angle TE and TM waves. IEEE Photonics J. Oct. 2021;13(5):1–7. doi: 10.1109/JPHOT.2021.3112550.
[23] Alhumairi MKA, Yahya SG, Azzawi IDJ, Al-Rubaiy AA. Experimental and computational investigation of flame holders in combustion chambers at different thermal loads. J Therm Eng. 2020;6(6):369–78. doi: 10.18186/THERMAL.833594.
[24] Elmnifi M, Mansur AN, Abdul-Ghafoor QJ, Alrubaiy A, Mustafa M, Khaleel M, et al. Induction heating for residential water desalination: A numerical simulation and experimental evaluation. Int J Heat Technol. 2023;41(6):1433–40. doi: 10.18280/ijht.410605.
[25] Zhdankin V, Ripperda B, Philippov AA. Particle acceleration by magnetic Rayleigh-Taylor instability: Mechanism for flares in black hole accretion flows. Phys Rev Res. 2023;5(4):043023.
[26] Hale N, Simonsen I, Brüne C, Kildemo M. Use of 4 × 4 transfer matrix method in the study of surface magnon polaritons via simulated attenuated total reflection measurements on the antiferromagnetic semiconductor MnF 2. Phys Rev B. 2022;105(10):104421.
[27] Yahya S, Azzawi IDJ, Abbas MK, Al-Rubaiy AAAG. Characteristics of acoustic drivers for efficient coupling to thermoacoustic machines. Lecture notes in engineering and computer science. 2019. p. 469–74.
[28] Orfanidis SJ. Electromagnetic waves and antennas. [Online]. http://eceweb1.rutgers.edu/%7eorfanidi/ewa/.
[29] Alwan ST, Mohamed WQ, Mahmood H. Effects of polymer thickness and frequency on the TE-mode using slab waveguide. In 2019 3rd International Symposium on Multidisciplinary Studies and Innovative Technologies (ISMSIT). IEEE; Oct. 2019. p. 1–10. doi: 10.1109/ISMSIT.2019.8932782.
[30] Li S-Q, Du CH, Han FY, Wang YD, Gao ZC, Tan YH, et al. Transverse magnetic modes of localized spoof surface plasmons. J Appl Phys. 2021;130(20):203104. doi: 10.1063/5.0067163.
[31] A. Nawi S, Mohamed MT, Rajab MA, Abd Ali Ghaidan A. Enhancing the performance of hybrid composites through the addition of zinc oxide and carbon fibers. Diyala J Eng Sci. Jun. 2024;17(2):112–9. doi: 10.24237/djes.2024.17208.